Department
of
APPLIED MATHEMATICS

A two-way nesting procedure for an ocean model with application to the Norwegian Sea.

by

Yngve Heggelund and Jarle Berntsen

Report no. 151 November 2000

UNIVERSITY OF BERGEN
Bergen, Norway

NB Rana
Depotbiblioteket

Department of Mathematics
University of Bergen
5008 Bergen
Norway

ISSN 0084-778x

A two-way nesting procedure for an ocean model with application to the Norwegian Ssea.

by

Yngve Heggelund and Jarle Berntsen

Report no. 151

November 2000

A two-way nesting procedure for an ocean model with application to the Norwegian Sea

Yngve Heggelund and Jarle Berntsen

23 August 2000

Abstract

Two-way nesting for a σ-coordinate ocean model is implemented. The test case is a traveling low pressure along the west coast of Norway. Different methods for interaction between the coarse grid and the fine grid have been investigated. It is found that both a Dirichlet type and a FRS-type boundary condition for the fine grid give reasonable results for this test case. The FRS-type boundary condition gives a smoother transition between the coarse and fine grid, but more noise in the interior of the fine grid. With no feedback from the fine grid to the coarse grid, phase differences between the solutions on the two grids cause unphysical vortices to be formed at the interface between the grids.

1 Introduction

Oceanic phenomena cover a wide range of spatial scales. To simulate small scale eddies or the flow around sharp topographic features and submerged installations or discharges of water requires a very fine mesh size. Because of the computational cost it will be prohibitive to cover the whole ocean with this fine mesh size in the foreseeable future. One way of overcoming this difficulty is to build hierarchies of nested models with focus on the area of interest. The success or failure of such efforts will depend both on the qualities of the basic ocean model and on the nesting technique. Conclusions on how nested models perform may depend on the choices of test problems. There is a growing literature describing nested models for the ocean. Major efforts include Spall and Holland (1991), Oey and Chen (1992), Fox and Maskell (1995), Fox and Maskell (1996), Laugier et al. (1996), Ginis et al. (1998), Blayo and Debreu (1999) and Rowley and Ginis (1999).

The nesting procedure should preferably conserve fluxes of mass, heat and momentum across the interfaces. In meteorology such a scheme was developed by Kurihara et al. (1979). Berger and Leveque (1998) have developed general adaptive mesh refinement algorithms for hyperbolic systems that also are conservative across interfaces. Ginis et al. (1998) applying the technique proposed by Kurihara et al. (1979) developed a nested primitive equation model that did not fictiously increase or decrease the transports of mass, momentum and heat through the dynamical interface. Rowley and Ginis (1999) included a mesh movement scheme in the nested ocean model and stated that mass, heat and momentum are conserved during the movement. The model applied in these two studies are based on the reduced gravity assumption so that the deep ocean is at rest below the active upper ocean, and the variables were discretized on nonstaggered grids. More general circulation models for the ocean often split the velocity field into external and internal modes and apply different time steps for the two modes, and staggered grids, typically B or C grids (Mesinger and Arakawa, 1976), are applied to reduce errors in the phase speeds. This complicates the bookkeeping of fluxes across mesh interfaces, and to our knowledge no nested ocean model based on mode splitting and staggered grids conserve fluxes across mesh interfaces (Spall and Holland, 1991; Oey and Chen, 1992; Fox and Maskell, 1995). Spall and Holland (1991) state that for short time integration this may not be critical whereas for climate studies conservation is most likely to be a critical issue.

Most papers describing nested ocean modelling efforts discuss stability problems and unsmooth solutions across the interfaces. Spall and Holland (1991) finding support in Zhang et al. (1986) state that it may be necessary to sacrifice exact conservation to obtain smooth, stable solutions. To stabilize

and smooth the solutions we find that combinations of horizontal and vertical diffusion, filtering the solutions in time and relaxation techniques or nudging are often applied. The present authors have in a recent paper (Heggelund & Berntsen, unpublished report, 2000), an eigenvector-eigenvalue problem, the stability properties of a two-way nested model for the linear shallow water equations. It is shown that even for very simplified subsets of equations enforcing conservation of volume will create instabilities in the purely hyperbolic case, and that some form for smoothing will be required to stabilize the solution.

The nesting described in for instance Spall and Holland (1991), Oey and Chen (1992) and Ginis et al. (1998) is two-way. In some studies data from previously run coarse grid models are used to drive fine grid models, see for instance (Svendsen et al., 1996; Berntsen and Svendsen, 1999). Fox and Maskell (1996) compared one-way and two-way nesting and concluded that using the model in one-way nesting mode resulted in more noise at the fine grid mesh boundaries with negligable decrease in computer time. In (Heggelund & Berntsen, unpublished report, 2000) it is shown that for the ideal purely hyperbolic case one-way nesting causes no stability problems as long as the method on each grid level is stable. However, if the solution at the fine grid is fed back to the coarse grid, one may expect a growth in energy unless some stabilizing techniques are applied.

In order to provide boundary condition for the fine grid, the coarse grid variables must be interpolated to the fine grid. There are numerous techniques that are potentially interesting for performing this task and some of these are considered recently by Alapaty et al. (1998). Based on studies with an idealized test case they conclude that zeroth-order interpolation may create large phase errors, quadratic interpolation may create overshooting and they suggest the use of advection equivalent interpolation schemes.

Nested model grids may be adaptive and movable or static. In order to follow evolving oceanic features such as wave fronts and propagating eddies it may be beneficial to apply for instance adaptive mesh refinement methods for hyperbolic systems described by Berger and Oliger (1984) or more recently by Berger and Leveque (1998). Blayo and Debreu (1999) have recently applied this technique to study the propagation of the barotropic modon and with a multilayered quasigeostrophic model. Rowley and Ginis (1999) in their model based on the reduced gravity assumption included a mesh movement scheme. However, as far as we know nested general circulation models with movable meshes have not yet been implemented. To run nested ocean models with large numbers of grid cells on each level is very CPU demanding and to allow the grids to evolve dynamically will add to the computational cost and the complexity of the coding.

Spall and Holland (1991) apply the same time step both on the coarse and the fine grid arguing that the coarse grid contributes little to the overall expense and that it would add an additional level of computational complexity for very little gain to have different time steps on the two grid levels. With equal Courant numbers on all levels the quality of the wave propagation relative to the mesh size will be approximately the same, and most of the more recent papers on nesting also refine the time step with the same factor as the spatial resolution keeping the Courant numbers constant.

A topic for debate in the literature on ocean model nesting is the degree of refinement from one level to the next. Grid ratios from 2:1 to 7:1 have been applied. Spall and Holland conclude that 3:1 and 5:1 ratios perform quite well, and even ratios of 7:1 are able to reproduce the solution reasonably well while the features are mostly contained within the fine region. To apply small ratios like 2:1, which is used for instance in Rowley and Ginis (1999), may force us to apply many grid levels before we achieve the resolution we would like to have in a given area. On the other hand large ratios may cause instabilities and unsmooth solutions across the interfaces.

There are numerous combinations of basic ocean models and nesting techniques that are potentially interesting and evidence on how such combinations perform is gradually growing as they are applied both to idealized test cases and to more realistic oceanic problems. The problems addressed so far range from advection of a simple cone, see Alapaty et al. (1998), through the popular barotropic modon and baroclinic vortex suggested by Spall and Holland (1991) to more realistic problems like the Norwegian Coastal Current described in Oey and Chen (1992).

The test case in the present report is in the latter category, and the coarse grid covers the Nordic Seas. Reviews of the main circulation in the Nordic Seas are recently given in Blindheim et al. (2000), Østerhus and Gammelsrød (1999) and Hansen and Østerhus (2000). Atlantic water enters the Norwegian Sea through the Faroe-Shetland Channel and between the Faroes and Iceland. The Atlantic inflow is to a large extent topographically steered. The shelf break is particularly steep in the Ormen Lange area at approximately 63.5°N, 5.0°E. In this area the depth varies from 200m to 1000m over approximately 30km with large local variations and sharp edges. Large velocities are also measured (Furnes 2000, pers.comm). On the shelf in this area the flow and the hydrography is determined by the Atlantic water masses and the Norwegian Coastal Current which flows northward along the coast of Norway from the Skagerrak to the Barents Sea (Hackett et al., 1995). There is a sharp surface front between the water masses with the coastal water lying above the Atlantic water. The front appears to generally follow the shelf break, but eddies and meanders are frequently ocurring (Haugan

et al., 1991; Hackett et al., 1995). Traveling atmospheric low pressures from south-west often hit the coast of Norway and create storm surges and these surges also create strong currents along the shelf break, see Martinsen et al. (1979). Both the topography, the variable forcing and the density fronts create phenomena that requires a very fine grid scale to resolve. The need for resolution is for instance pointed out in Hacket et al. (1995) and Böning and Budich (1992). This area is of particular interest now because a major gas field has been discovered and also named Ormen Lange. Development of this field is under planning with installations at approximately 1000m depth. To be able to estimate the drag of waves and currents on submerged installations like risers to platforms and pipelines, best possible knowledge about the currents and not least their variability should be acquired. In our studies with nested ocean models for the Norwegian Sea we have chosen to focus on the Ormen Lange area both because a high spatial resolution is required to model the physical oceanography along the shelf break and because of the growing industrial interest in the area.

The basic ocean model is the 3-dimensional σ-coordinate model described in (Berntsen, 2000). The nesting is static with a grid ratio of 5:1 and the same ratio is also applied to the time steps. Experiments with both one and two-way nesting are performed, and various techniques for coupling between the two grids are also tested. The circulation along the shelf break is forced with the traveling storm described in Martinsen et al. (1979).

2 The basic equations

The basic equations are the Reynolds momentum equations. It is assumed that the weight of the fluid identically balances the pressure (hydrostatic approximation). The following equations describe the variables as functions of the Cartesian coordinate system (x, y, z).

The continuity equation is

$$\nabla \cdot \vec{U} + \frac{\partial W}{\partial z} = 0 \tag{1}$$

and the Reynolds momentum equations are

$$\frac{\partial U}{\partial t} + \vec{U} \cdot \nabla U + W\frac{\partial U}{\partial z} - fV = -\frac{1}{\rho_0}\frac{\partial P}{\partial x} + \frac{\partial}{\partial z}(K_M \frac{\partial U}{\partial z}) + F_x \tag{2}$$

$$\frac{\partial V}{\partial t} + \vec{U} \cdot \nabla V + W\frac{\partial V}{\partial z} + fU = -\frac{1}{\rho_0}\frac{\partial P}{\partial y} + \frac{\partial}{\partial z}(K_M \frac{\partial V}{\partial z}) + F_y \tag{3}$$

$$\rho g = -\frac{\partial P}{\partial z} \tag{4}$$

In addition there are conservation equations for temperature and salinity;

$$\frac{\partial T}{\partial t} + \vec{U} \cdot \nabla T + W\frac{\partial T}{\partial z} = \frac{\partial}{\partial z}(K_H \frac{\partial T}{\partial z}) \tag{5}$$

$$\frac{\partial S}{\partial t} + \vec{U} \cdot \nabla S + W\frac{\partial S}{\partial z} = \frac{\partial}{\partial z}(K_H \frac{\partial S}{\partial z}) \tag{6}$$

No explicit horizontal diffusion is applied. The density is computed according to an equation of state of the form

$$\rho = \rho(S, T) \tag{7}$$

taken from Wang (1984) .

The horizontal eddy viscosity terms F_x and F_y may be written

$$F_{x,y} = \frac{\partial}{\partial x}(A_M \frac{\partial(U,V)}{\partial x}) + \frac{\partial}{\partial y}(A_M \frac{\partial(U,V)}{\partial y}) \tag{8}$$

The horizontal diffusivities, A_M, are computed according to Smagorinsky (1963) .

$$A_M = C_M \Delta x \Delta y \frac{1}{2}[(\frac{\partial U}{\partial x})^2 + \frac{1}{2}(\frac{\partial V}{\partial x} + \frac{\partial U}{\partial y})^2 + (\frac{\partial V}{\partial y})^2]^{\frac{1}{2}} \tag{9}$$

In this study C_M is set to 0.2.

The vertical viscosity/diffusivity parameters K_M and K_H are computed according to the Mellor & Yamada 2 1/2 turbulence closure scheme (Mellor and Yamada, 1982).

3 The numerical method

The system of equations (1)-(9) form a set of simultaneous partial differential equations. These are solved numerically using a σ-coordinate ocean model (Berntsen, 2000). The horizontal scheme is staggered using the C-grid (Mesinger and Arakawa, 1976), so the velocities and transports are given at cell interfaces and the other variables are given at cell centers.

The method of fractional steps is applied. That is a sequence of subroutines is called to perform specific subtasks and update the variables. After all the subroutines are called, the effect of all terms in the governing equations are included. The scalar fields S and T are advected with the TVD scheme with the superbee limiter (Sweby, 1984).

Mode splitting is also used. This means that the $2D$ fields, i.e. the transports and the surface elevation are propagated with a shorter time step than the other variables. The advantage is that the CFL criterion corresponding to fast surface waves (the external mode) does not restrict the time step for the $3D$ internal mode which then can be propagated with a larger time step.

4 The nesting procedure

Two different methods of coupling the two grids have been tested. The methods share the same procedure for updating the coarse grid variables from the fine grid solution, but they differ in the transfer of information from the coarse grid to the fine grid.

4.1 Method 1: Dirichlet boundary condition for the fine grid

A portion of the nested grid is shown in Figure 1. Around the refined region, two additional fine grid cells are placed. Boundary values for the fine grid are prescribed to the points denoted by 'input interface' in Figure 1 as a Dirichlet boundary condition. Inside the refined region, both a coarse grid and a fine grid solution exist, and after the solution on the fine grid is stepped in time the coarse grid field values on and inside of the feedback interface are updated from the fine grid solution. This is basically the same coupling procedure used by Fox and Maskell (1995) and Spall and Holland (1991) .

According to Spall and Holland (1991), it is important to separate the input interface and the feedback interface to decrease the noise in the solution. This means that the points where boundary values for the fine grid is specified should not be used to update the coarse grid solution. However, they

also found that this separation should remain small in order to maximize the information available from the fine grid solution.

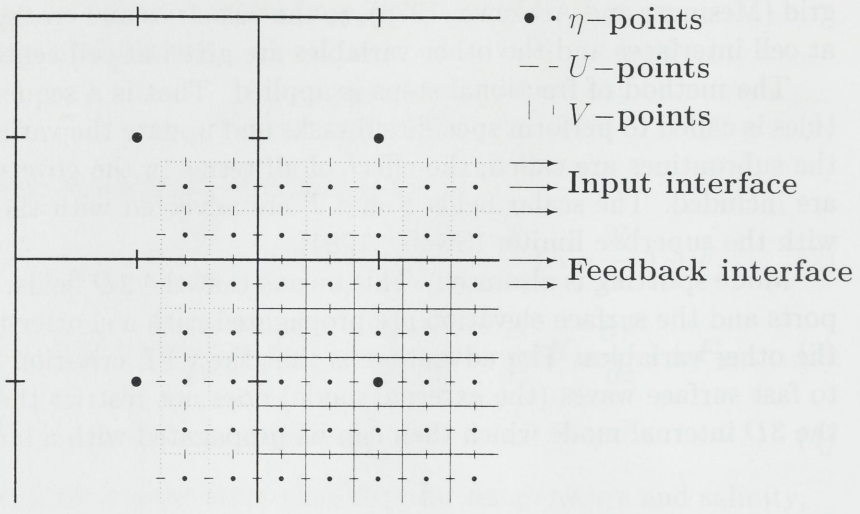

Figure 1: Portion of the nested grid seen from above. The coarse grid points are denoted by large symbols, and fine grid points with small symbols.

4.2 Method 2: FRS-zone technique in the coupling

As an alternative to specifying the boundary condition for the fine grid as a Dirichlet boundary condition, the values in a 7 cell wide zone near the fine grid boundary are relaxed towards the coarse grid solution using the FRS-zone open boundary technique (Martinsen and Engedahl, 1987). As in method 1, the solution on the fine grid on and inside the feedback interface is used to update the coarse grid solution, see Figure 2.

Let $i = 1 \ldots 7$ be an index of a cell in the FRS-zone, starting with the outermost. Let $\tilde{X}_i^{n+1}$ be the calculated fine grid value in the FRS-zone, and let $\hat{X}_i^{n+1}$ be an interpolation of coarse grid values to the same grid cell. The new value X_i^{n+1} is then given through a forcing term of the form

$$\frac{X_i^{n+1} - \tilde{X}_i^{n+1}}{\Delta t} = \kappa_i (\hat{X}_i^{n+1} - X_i^{n+1}), \tag{10}$$

where κ_i is given and is independent of the time step, but can depend on i.

Equation (10) can also be written as

$$X_i^{n+1} = \alpha_i \hat{X}_i^{n+1} + (1 - \alpha_i)\tilde{X}_i^{n+1}, \tag{11}$$

where

$$\alpha_i = \frac{\Delta t \kappa_i}{1 + \Delta t \kappa_i}.$$

Equation (11) is the form used in the numerical code.

In the current study, the strength of the forcing, κ_i, is chosen so that $\alpha_i = 1 - \tanh\frac{i-1}{2}$ for $\Delta t = \Delta t_{E0}$, where Δt_{E0} is approximately the time step required to resolve the fast surface waves ($\Delta t_{E0} \approx \frac{\Delta x}{\sqrt{2gH_{\max}}}$). From our experience, this is a reasonable setting for the forcing term.

The algorithm for constructing α_i, then becomes

1. $\beta_i = 1 - \tanh\frac{i-1}{2}$
2. $\kappa_i = \frac{\beta_i}{\Delta t_{E0}(1-\beta_i)}$
3. $\alpha_i = \frac{\Delta t \kappa_i}{1+\Delta t \kappa_i}$

Expression (11) is given in Martinsen and Engedahl (1987), and they show that it is equivalent to Equation (10). They do not, however, mention that by fixing the α's, the forcing in the FRS-zone will vary with Δt. The above algorithm ensures that the forcing stays constant for all Δt.

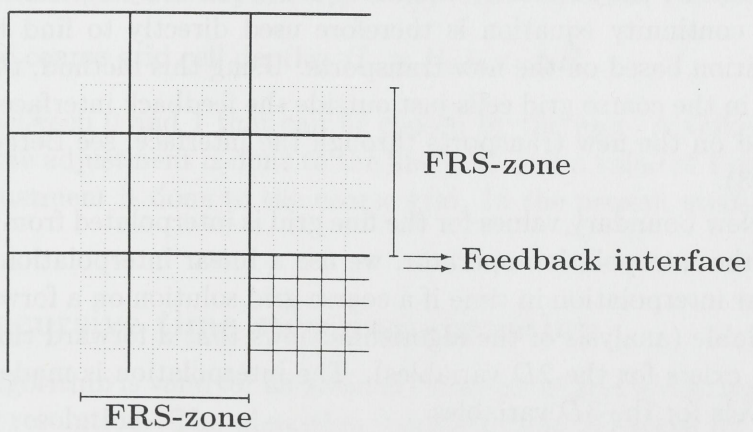

Figure 2: Portion of the nested grid seen from above. The values in the FRS-zone are updated based on interpolated coarse grid values. For clarity, the U, V and η points are not shown.

4.3 The feedback to the coarse grid

In the feedback of the fine grid solution to the coarse grid, we have implemented an option of 'forcing' the coarse grid values towards averages of corresponding fine grid values. Let $\tilde{X}_C$ denote a coarse grid value, and let $\bar{X}_f$ denote the average of corresponding fine grid values. The updated coarse grid value, X_C, is then given by

$$X_C^n = (1 - D)\tilde{X}_C^n + D\bar{X}_f^n. \tag{12}$$

$D = DT \cdot \gamma$, where γ is the inverse of a time scale and DT is the time step. The time scale can range between DT and ∞. D can therefore have a value between 0 (no feedback) and 1 (instantaneous feedback).

This method of 'forcing' has also been used by Kurihara and Bender (1980). It was found to increase stability for two-way nested shallow water equations (Heggelund & Berntsen, unpublished report, 2000), and is therefore implemented as an option here.

4.4 Restriction and interpolation operators

The restriction operator used is a straightforward average value, where the average is taken along constant z levels for the $3D$ variables. An exception is made for the surface elevation, in order to satisfy the continuity equation. The continuity equation is therefore used directly to find the new surface elevation based on the new transports. Using this method, the surface elevation in the coarse grid cells just outside the feedback interface is also updated based on the new transports through the interface, see Berger and LeVeque (1998).

New boundary values for the fine grid is interpolated from the coarse grid. For the interpolation operator, we use a linear interpolation in space and a linear interpolation in time if a coarse grid solution on a forward time step is available (analysis of the algorithm shows that a forward time step solution only exists for the $2D$ variables). The interpolation is made along constant z levels for the $3D$ variables.

A linear interpolation of the transports conserves the fluxes through the interface between the grids. Together with the above mentioned restriction of the surface elevation, the nesting technique maintains global and local volume conservation. Mass and energy conservation is not necessarily achieved by this method. However, for short time simulations this may not be so critical.

4.5 Adjustments of the depth matrixes

The 20 km depth matrix and the 4 km depth matrix are taken from two different databases. Beacuse of this the depth of a 20 km grid cell may not be exactly equal to the 25-point average of corresponding 4 km grid cells. Some adjustments of the depth matrixes are therefore necessary.

For simplicity, the land matrix in the fine grid is modified so that all the fine grid cells corresponding to a coarse grid wet cell are wet cells, and all land cells corresponding to a coarse grid land cell are land cells. This simplifies the mass conservation properties near land, and the modification probably has very little impact on the solution away from the coast.

A necessary condition for achieving mass and volume conservation is that the volume of the coarse grid cell columns are equal to the volume of the integral of fine grid cell depths in the overlap. Therefore, the depth matrixes for the coarse and fine grid are adjusted, so that the 25-point average depth of the fine grid equals the corresponding coarse grid depth. This is done according to the following algorithm for each coarse grid cell in the overlapping region.

1. Calculate the 25-point average depth, H_f, of fine grid depths, $h_{f,i}$, $H_f = \frac{1}{25}\sum_i h_{f,i}$.

2. Compute $\Delta H = H_f - H_c$, where H_c is the depth of the corresponding coarse grid cell.

3. Adjust the fine grid cell depths; $h_{f,i} = h_{f,i} - (1-c)\cdot\Delta H$, $i = 1\ldots25$.

4. Adjust the coarse grid cell depths; $H_c = H_c + c\cdot\Delta H$.

c is a number between 0 and 1 that can be chosen by the user. A value of 0 means that all the adjustment is done to the fine grid, and a value of 1 means that all the adjustment is done to the coarse grid. In the present study c is set to 0.5.

4.6 The recursive time stepping algorithm

The following algorithm is valid for an arbitrary number of grid levels, `ngrid`, with increasing resolution. The algorithm calculates `n2d` $2D$-steps for grid `ig` before taking a $3D$-step. The number of $2D$-steps calculated for grid `ig` is stored in the variable `num2d(ig)`. It is assumed that the time step ratio between the different refinements is 1 : 5.

The main program (4.1) calls the recursive procedure `solve` (4.2), which in turn solves the $2D$ and $3D$ part of the equations on all grids. `solve2d`

solves the $2D$ barotropic part of the equations and `solve3d` includes all other terms (nonlinear effects, advection of scalar fields, internal pressure effects etc).

Program 4.1 The main program

```
Initialize all field variables
ig = 1
num2d(1:ngrid) = 0
do istep3d = 1,numstep
   do istep2d=1,n2d
      call solve(ig)
   end do
end do
```

5 Application: Storm passage in the Norwegian Sea

5.1 Description of the test case

Traveling atmospheric low pressures from the south-west often occur in the Norwegian Sea, especially during the autumn months. The effects of these on the sea level variations and the currents have earlier been studied both analytically and numerically in Martinsen et al. (1979), using a $2D$ numerical model and simplified bathymetry. Other papers on the effects of storm surges include Gjevik (1991) and Gjevik and Røed (1976) .

The bathymetry of the area is given in Figure 3. Along the coast of Norway is a narrow shelf, and the shelf edge is very sharp. Long barotropic waves are trapped to the shelf or the coastal boundary after a storm passage. There are also large local variations in the bathymetry which can cause strong local variations to the currents. The local variations are of special interest to oil and gas companies because a large gas field has been discovered at the shelf break, named Ormen Lange. Installations are planned at approximately 1000 m depth, and there is a need for knowledge about the currents and their variability at this location. The region marked with the dash-dot lines in Figure 3 has therefore been refined with a 4 km grid resolution, while a 20 km resolution has been used for the rest of the area shown.

Figure 4 shows an enlargement of the fine grid region. Four positions are marked ol1-ol4. These are approximate positions of real moorings. The

Program 4.2 The recursive algorithm solve

```
num2d(ig) = num2d(ig) + 1
call solve2d(ig)
if (ig>1) then
   update 2d boundary values for fine grid
endif
if (ig<ngrid) then
  do i=1,5
     call solve(ig+1)
  end do
endif
if (ig<ngrid) then
   update 2d coarse grid values in fine grid overlap
endif
!
if (mod(num2d(ig),n2d)==0) then
   call solve3d(ig)
   if (ig>1) then
      update 3d boundary values for fine grid
   endif
   if (ig<ngrid) then
      update 3d coarse grid values in fine grid overlap
   endif
   num2d(ig) = 0
endif
```

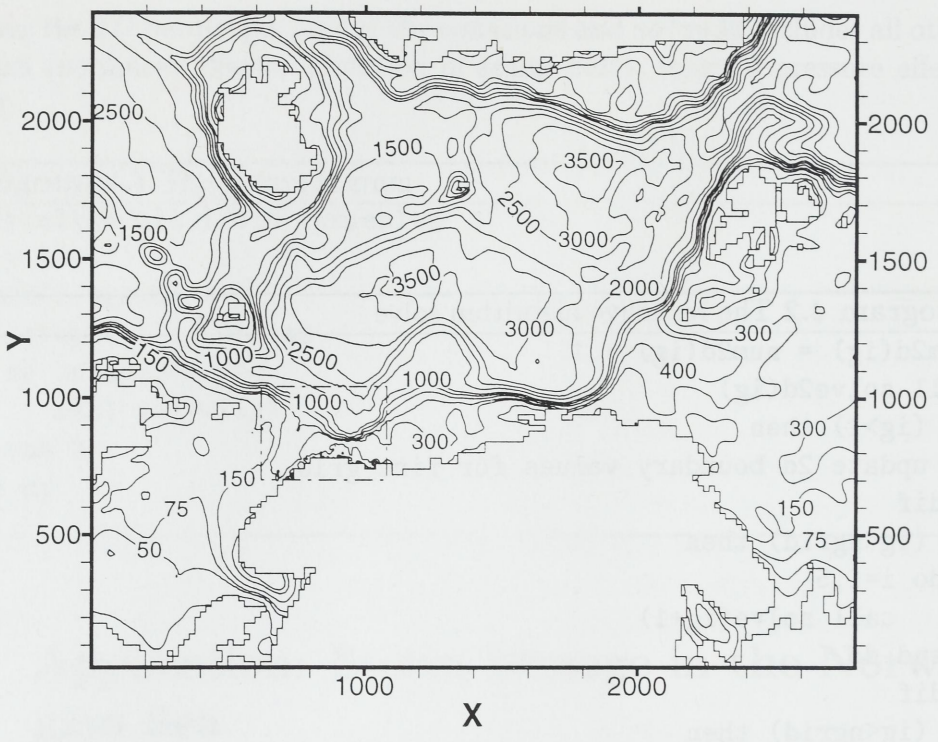

Figure 3: The bottom matrix. The refined area is outlined with the dash-dot lines. The axis give the distance from the lower left corner in units of kilometers.

model calculated field values at these positions are stored every time step at 10 m and 50 m above the bottom.

In order to study the effects of storms in this nested $3D$ model, the same traveling storm used in Martinsen et al. (1979) has been implemented here. A propagating pressure disturbance is given by

$$p(x, y, t) = p_0(t) \exp\{-[(x - x_0 - u_0 t)^2 + (y - y_0 - v_0 t)^2]/R^2\}, \qquad (13)$$

where x_0, y_0 is the initial position of the center of the pressure disturbance, and u_0 and v_0 are the x and y components of the propagation velocity. The wind velocity components u_g and v_g are given by

$$u_g = -\frac{\sigma}{f \rho_a} \frac{\partial p}{\partial y} \qquad (14)$$

$$v_g = \frac{\sigma}{f \rho_a} \frac{\partial p}{\partial x} \qquad (15)$$

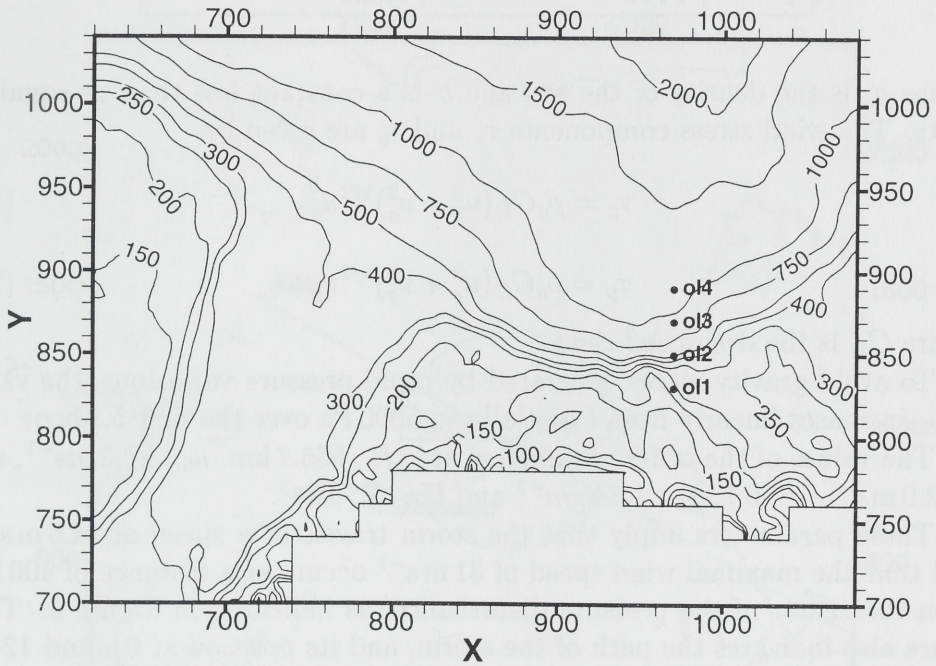

Figure 4: The bottom matrix in the refined region. Four mooring stations are marked and named ol1-ol4.

Table 1: Different methods of interaction between the coarse and the fine grid

Setup	Coarse to fine grid	Fine to coarse grid
0	N/A	N/A
1	Dirichlet	Instantaneous
2	FRS	Instantaneous
3	Dirichlet	'Forced' (3000 s)
4	FRS	'Forced' (3000 s)
5	Dirichlet	None
6	FRS	None

where ρ_a is the density of the air, and σ is a constant less than or equal to unity. The wind stress components τ_x and τ_y are given by

$$\tau_x = \rho_a C_D (u_g^2 + v_g^2)^{1/2} u_g \tag{16}$$

$$\tau_y = \rho_a C_D (u_g^2 + v_g^2)^{1/2} v_g \tag{17}$$

where C_D is the drag coefficient.

To avoid gravity waves generated by rapid pressure variations, the value of p_0 increases linearly from 0 initially to 5000 Pa over the first 5.5 h.

The values of the other parameters are: R : 565.7 km, u_0 : 21.5 $\mathrm{m}s^{-1}$, v_0 : $-12.0\,\mathrm{m}s^{-1}$, σ : 0.7, ρ_a : 1.3 $\mathrm{kg}m^{-3}$ and C_D : $3 \cdot 10^{-3}$.

These parameters imply that the storm travels at a speed of 24.6 $\mathrm{m\,s}^{-1}$, and that the maximal wind speed of 31 $\mathrm{m\,s}^{-1}$ occurs at a distance of 400 km from the center of the pressure disturbance, as indicated in Figure 5. This figure also indicates the path of the storm, and its position at 0 h and 12 h.

The time step used for the coarse grid $2D$ mode is 37.5 s and for the $3D$ mode 600 s. The respective time steps on the refined grid are 1/5 of these in order to conserve the Courant number.

All the simulations were started with zero velocities and zero surface elevation, and were run for 48 h. Six runs were made with different methods for interaction between the coarse and the fine grid. The setups are given in Table 1. The degrees of freedom chosen were either Dirichlet or FRS-zone methods in the coupling from the coarse grid to the fine as explained in Section 4.1 and 4.2, and three alternatives of feeding back the fine grid solution to the coarse grid as explained in Section 4.3. Setup 0 refers to an unrefined 20 km model.

Time series of the sea elevation at Kristiansund (see Figure 5 for location) are given in Figure 6. The results for the different setups are more or less

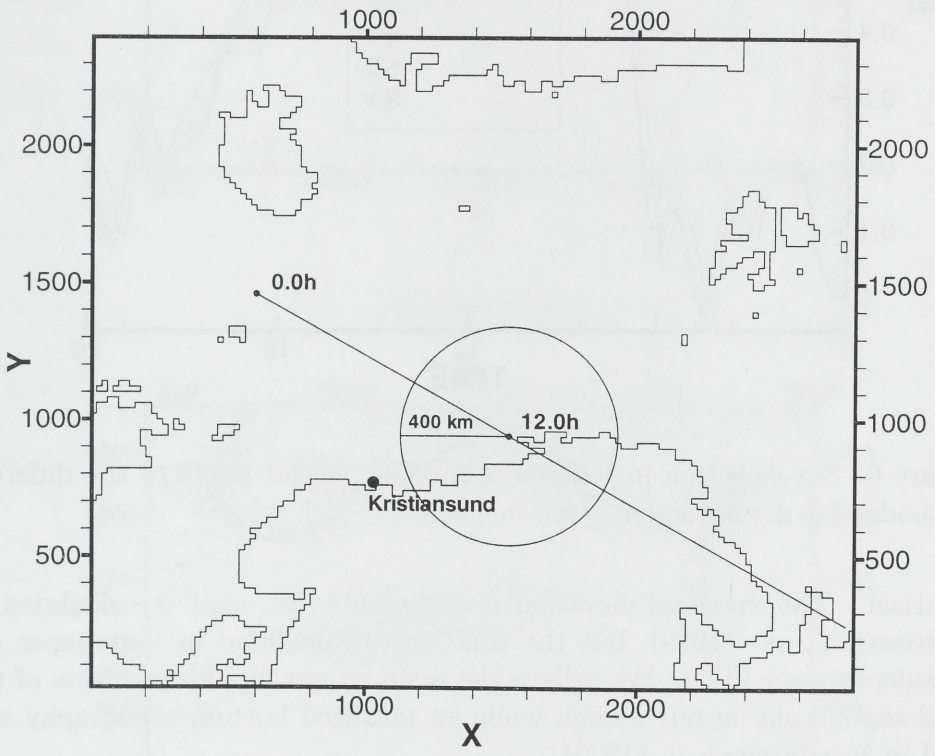

Figure 5: Schematic overview of the storm passage.

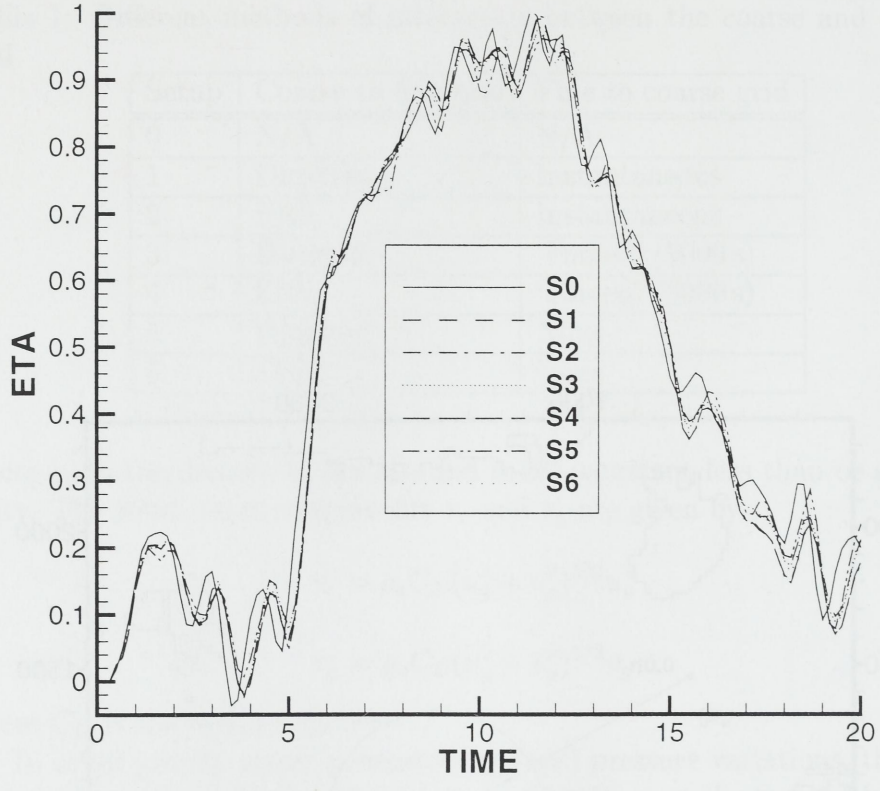

Figure 6: Sea elevation in Kristiansund. The legend refers to the different methods of grid interaction given in Table 1

identical. The maximal elevation is comparable to what is calculated in Martinsen et al. (1979), but the time series calculated in that paper are considerably smoother. We believe the main reason for this is effects of the local topography in our model, while an idealized bottom topography was used in Martinsen et al. (1979).

Figure 7 shows the sea elevation after 12 h from the 20 km model (setup 0) and from setup 1 in Table 1. The signal seems to cross the interface of the fine grid without any disturbance, so the features of the surface elevation are well preserved on the fine grid. This was also true for all the other grid interactions in Table 1. As in Martinsen et al. (1979), the contours run nearly parallel and equally spaced on the shelf, which shows that the sea level decreases nearly linearly over the shelf. The apparent increase in variability in the coarse grid portion of the nested model (Figure 7(b)) is artificial and is due to interpolation 'errors' in the plotting.

After 48 h the differences between the 20 km model and the nested models

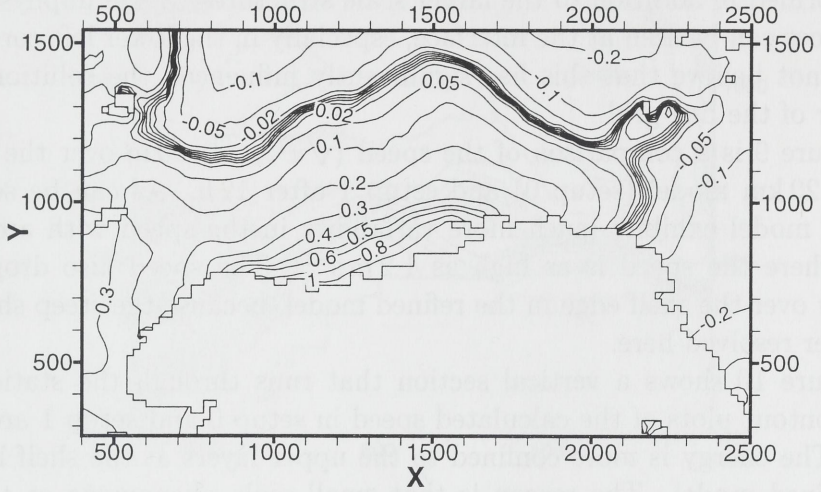

(a) 20 km model

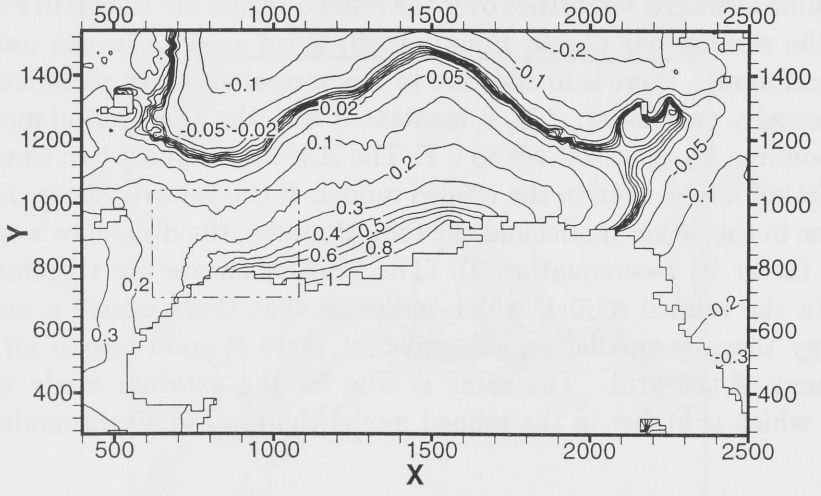

(b) Refined model setup 1

Figure 7: Comparison of the sea elevation after 12 h.

become more apparent. Figure 8 shows the sea elevation around the refined region at this time. In the refined region of the nested model, more variability can be seen than in the 20 km model. Small topographic eddies have been formed in addition to the larger scale structures. Some unphysical disturbances can be seen at the interface, especially in the lower left corner, but we do not believe that this has significantly influenced the solution in the interior of the fine grid.

Figure 9 is a comparison of the speed ($\sqrt{u^2+v^2}$) 10 m over the bottom in the 20 km model (setup 0) and setup 1 after 12 h. As can be seen, the refined model exhibits much more variability in the speed with areas near land where the speed is as high as $1.2\,\mathrm{m\,s^{-1}}$. The speed also drops more sharply over the shelf edge in the refined model, because the steep shelf edge is better resolved here.

Figure 10 shows a vertical section that runs through the stations ol1-ol4. Contour plots of the calculated speed in setup 0 and setup 1 are shown here. The energy is more confined to the upper layers at the shelf break in the refined model. The reason is that small scale phenomena at the shelf break are better represented on the fine grid. On the coarse grid the energy associated with these un-resolvable small scale phenomena is instead mixed down to lower layers.

Volume averaged viscosities over the refined region are shown in Figure 11. In all the simulations C_M in Equation (9) is set to 0.2. In the mode split numerical model, there is in addition to the normal viscosity parameter, AM, a $2D$ viscosity parameter, AM_{2D}, associated with the $2D$ external mode. The corresponding C_{M2D} is also set to 0.2. The AM's are almost two times larger in the 20 km model than in the refined model. If the velocity shears had been the same in the 20 km model and the refined model, the difference would have been a factor 25 (see equation 9). The velocity shears are therefore much larger in the refined model, which indicates that there is still a movement of energy towards smaller scales, and that there is good reason for further refinement of the grid. The same is true for the external mode viscosity, AM_{2D}, which is higher in the refined model than in the 20 km model.

5.2 One-way vs. two-way nesting

A comparison of the calculated speeds at the mooring stations ol1 and ol4 for the 20 km model, one-way (setup 5) and two-way (setup 1) nesting is given in Figure 12. A noticeable feature is that the amplitude of the speed using one-way nesting is considerably higher than in the unrefined model. The speed in the two-way nested model is closer to the speed in the unrefined model, especially at ol4. One reason for the higher speed in the one-way nested

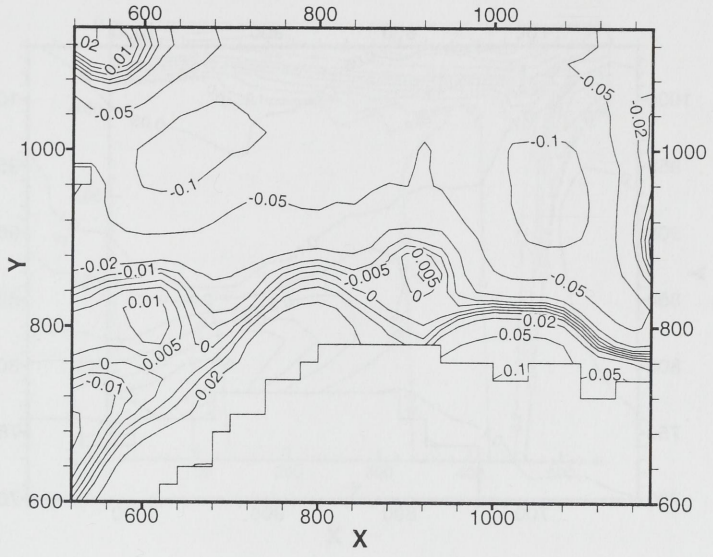

(a) 20 km model

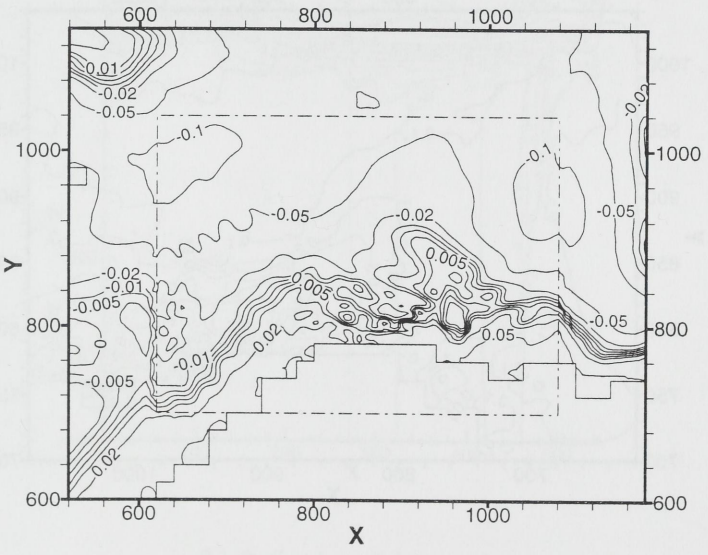

(b) Refined model setup 1

Figure 8: Comparison of the sea elevation after 48 h.

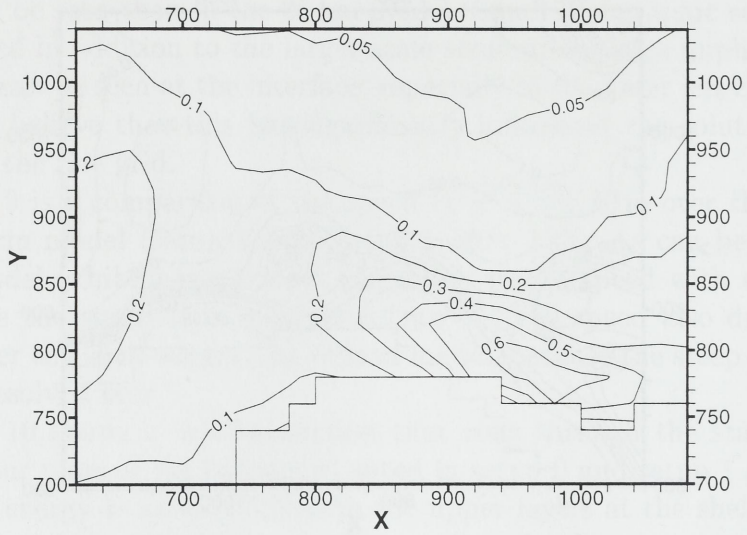

(a) 20 km model

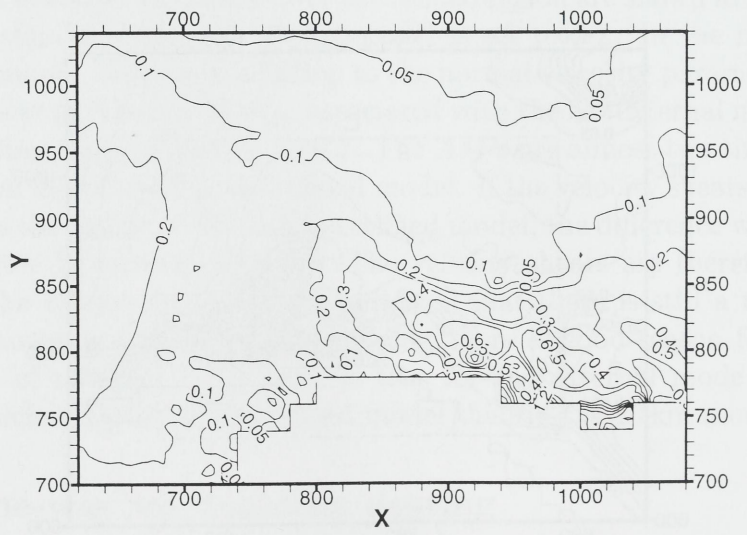

(b) Refined model setup 1

Figure 9: Comparison of velocity 10 m over the bottom after 12 h.

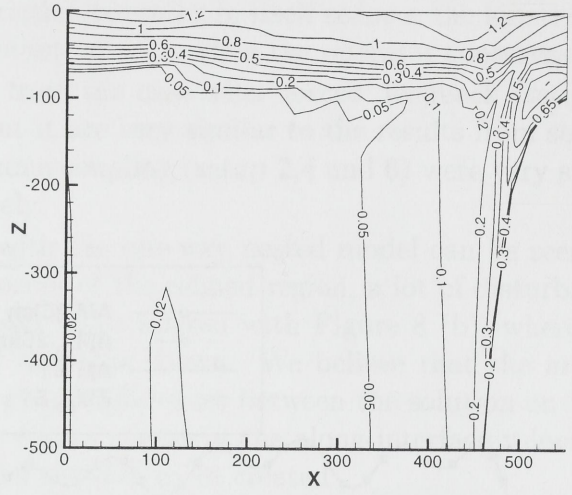

(a) 20 km model

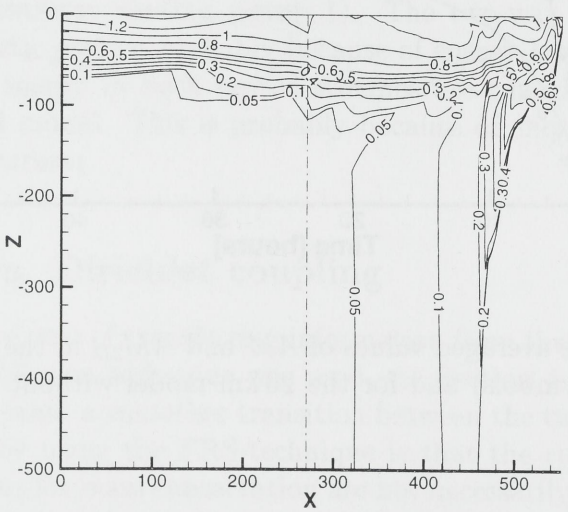

(b) Refined model setup 1

Figure 10: Vertical section of speed after 12 h. The units on the horizontal axis is in km, while the vertical axis is in m The interface of the refined region is marked with the dash-dot line.

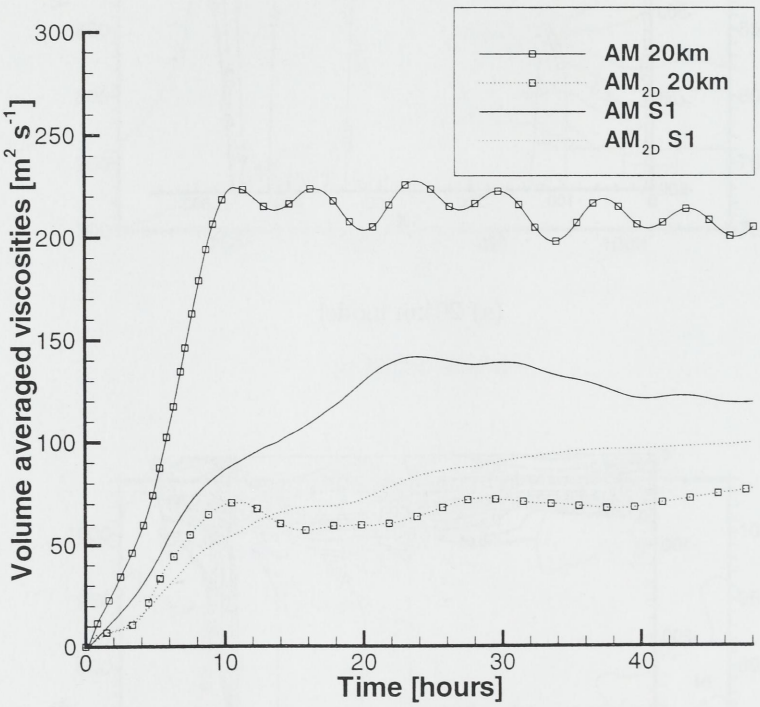

Figure 11: Volume averaged values of AM and AM_{2D} in the fine grid region for Setup 1 (no symbols) and for the 20 km model without nesting (square symbols).

model is that phase differences between the fine grid and the coarse grid may cause reflection of energy at the interface between the grids. Another reason is that the restriction operator in itself reduces the kinetic energy, except for the case of constant velocity when the operator conserves energy.

The results from the case with 'forced' feedback (setup 3) is not shown in Figure 12, but it are very similar to the results from setup 5. The results from the FRS-zone coupling (setup 2,4 and 6) were very similar to setup 1,3 and 5 respectively.

A problem with the one-way nested model can be seen in Figure 13. In the lower left corner of the refined region, a lot of disturbances can be seen. This figure should be compared with Figure 8 (b), where the result of the two-way nested model is shown. We believe that the main reason for the disturbances is phase differences between the solution on the coarse and the fine grid, which causes shears in the along-interface velocities. This in turn causes unphysical vortices to be created.

In a recent report (Heggelund & Berntsen, unpublished report, 2000), it was found that some two-way nesting schemes for the shallow water equations were unstable. Looking at Figure 14, this does not seem to be as much of a problem with the full set of equations, because of the dissipation terms. There is very little difference in the energy development between one-way (setup 5) and two-way nesting (setup 1). The two-way nested model has slightly less kinetic energy, probably because of energy lost in the restriction operator. The energy in both nested schemes are considerably lower than in the unrefined model. This is probably because of energy lost due to the interpolation operator.

5.3 FRS vs. Dirichlet coupling

As an alternative way of transferring information from the coarse grid to the fine grid, an FRS-zone technique was used, see Section 4.2. This technique was believed to cause a smoother transition between the two grids. However, a price to pay by using the FRS-technique is that the continuity equation and the equations for mass conservation are not necessarily valid in the FRS-zone. We believe that this is the cause of the disturbances in the interior of the refined region in Figure 15. On the other hand, the transition over the interface is smoother. In particular the disturbances that could be seen in the lower left corner with setup 1 (Figure8 (b)) have now been reduced.

The other results from the FRS-zone technique are not shown in this report. They are very similar to the results from the Dirichlet coupling, except from the increased noise mentioned above.

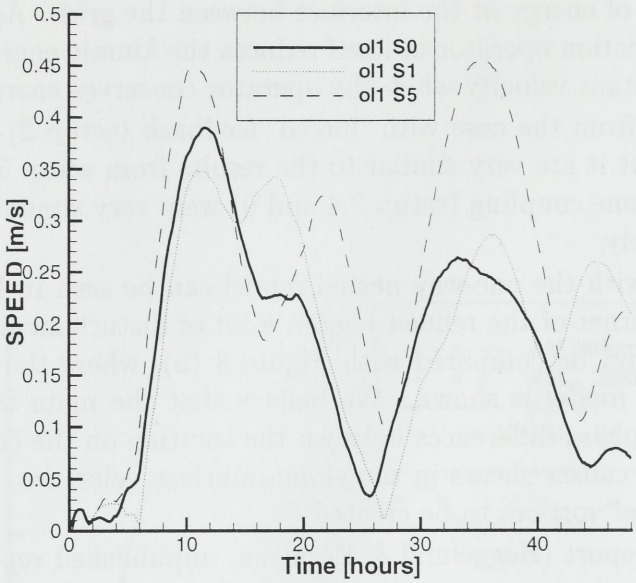

(a) Station ol1

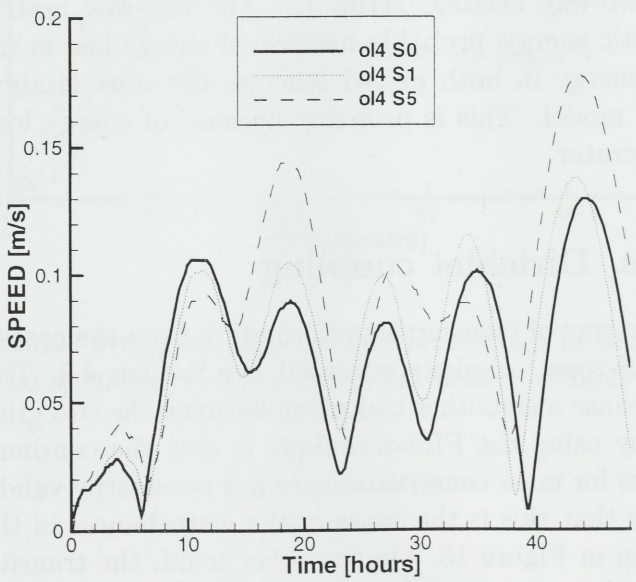

(b) Station ol4

Figure 12: Speed at station ol1 and ol4.

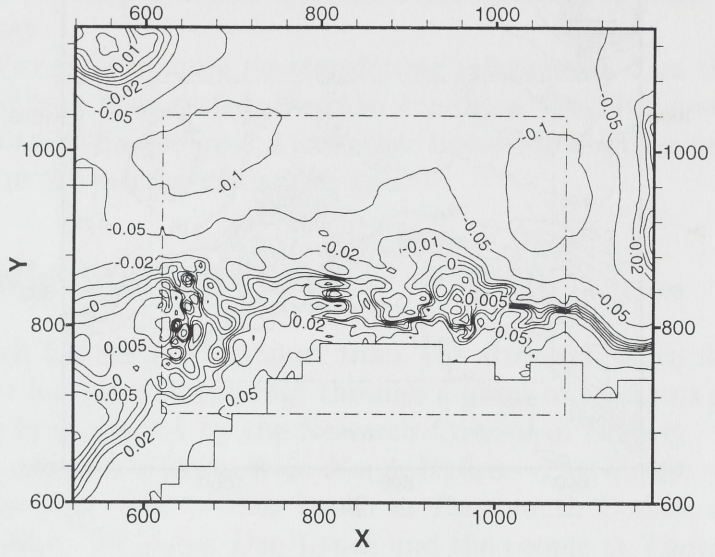

Figure 13: Surface elevation at 48 hours for setup 5.

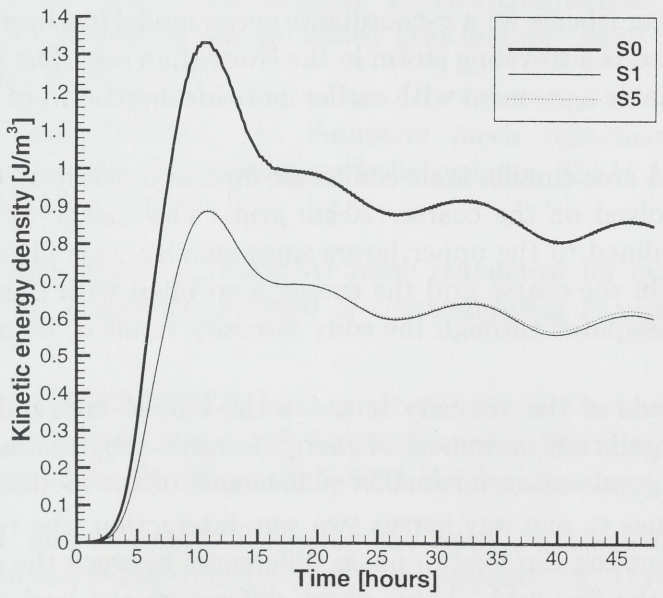

Figure 14: Energy densities in the refined grid area.

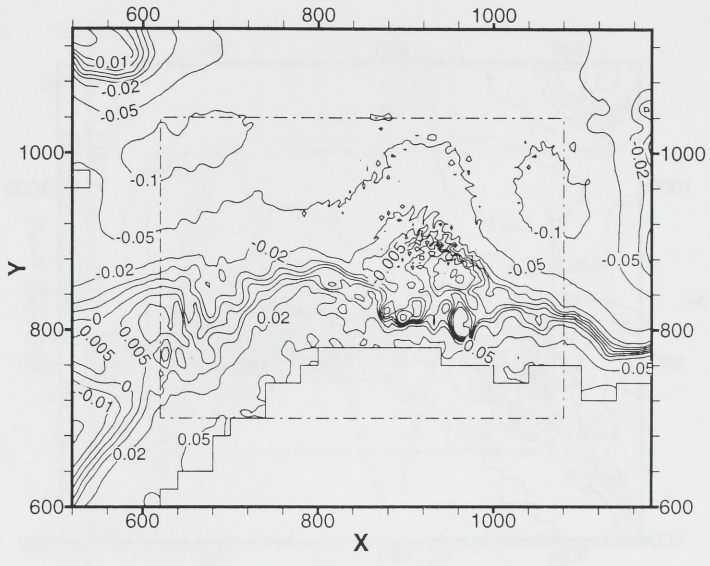

Figure 15: Surface elevation at 48 hours for setup 2.

6 Conclusion

A two-way nesting scheme for a σ-coordinate ocean model has been described. The test case used is a traveling storm in the Norwegian sea. The model gives results in reasonable agreement with earlier more idealized studies (Martinsen et al., 1979).

In the refined area smaller scale eddies are formed in addition to phenomena already resolved on the coarser 20 km grid. The energy in the refined grid is more confined to the upper layers since smaller scale phenomena are resolved here. On the coarse grid the energy associated with these phenomena has to be dissipated through the eddy viscosity terms or be mixed down to lower layers.

The magnitude of the viscosity terms in the refined area indicates that there is still a significant movement of energy towards subgrid scale phenomena, so there is good reason for further refinements of the model.

When it comes to one way versus two way interaction, the results show that one way coupling can lead to phase differences between the solution on the coarse and the fine grid. These phase differences can lead to unphysical disturbances at the interface between the grids. These disturbances are significantly reduced with a two way coupling. The speeds at the measuring stations ol1-ol4 are significantly larger in one way coupling versus two way.

One reason is reflection of energy at the interface because of phase differences. Another reason is that the restriction operator in itself reduces the kinetic energy.

Two different techniques for transferring information from the coarse to the fine grid have been tested; Dirichlet condition and FRS-zone technique. The FRS-zone technique gave a smoother transition over the interface, but more noise in the interior of the fine grid.

Acknowledgments

This research has received support from The Research Council of Norway (Programme for Supercomputing) through a grant of computing time. The first author is supported by the Research Council of Norway. The second author has received support from Norsk Hydro. This report was written during a one year visit to Dan Lynch at Dartmouth College in Hanover, New Hampshire. We thank Dan Lynch and the people at Thayer School of Engineering, Dartmouth College for their hospitality.

References

Alapaty, K., Mathur, R., and Odman, T., Intercomparison of spatial interpolation schemes for use in nested grid models, *Mon. Wea. Rev.*, 126, 243–249, 1998.

Berger, M. and Leveque, R., Adaptive mesh refinement using wave-propagation algorithms for hyperbolic systems, *SIAM J. Numer. Anal.*, 35, 2298–2316, 1998.

Berger, M. and Oliger, J., Adaptive mesh refinement for hyperbolic partial differential equations, *Journal of Computational Physics*, 53, 484–512, 1984.

Berntsen, J., USERS GUIDE for a modesplit σ-coordinate numerical ocean model, Technical Report 135, Dept. of Applied Mathematics, University of Bergen, Johs. Bruns gt.12, N-5008 Bergen, Norway, 2000, 48p.

Berntsen, J. and Svendsen, E., Using the Skagex dataset for evaluation of ocean model skills, *Journal of Marine Systems*, 18, 313–331, 1999.

Blayo, E. and Debreu, L., Adaptive mesh refinement for finite-difference ocean models: First experiments, *Journal of Physical Oceanography*, 29, 1239–1250, 1999.

Blindheim, J., Borovkov, V., Hansen, B., Malmberg, S., Turrell, W., and Østerhus, S., Upper layer cooling and freshening in the norwegian sea in relation to atmospheric forcing, *Deep-Sea Research I*, 47, 655–680, 2000.

Böning, C. and Budich, R., Eddy dynamics in a primitive equation model: Sensitivity to horizontal resolution and friction, *Journal of Physical Oceanography*, 22, 361–381, 1992.

Fox, A. and Maskell, S., Two-way interactive nesting of primitive equation ocean models with topography, *Journal of Physical Oceanography*, 25, 2977–2996, 1995.

Fox, A. and Maskell, S., A nested primitive equation model of the iceland-fareoe front, *Journal of Geophysical Research*, 101, 18259–18278, 1996.

Ginis, I., Richardson, R., and Rothstein, L., Design of a multiply nested primitive equation ocean model, *Mon. Wea. Rev.*, 126, 1054–1079, 1998.

Gjevik, B., Simulations of shelf sea responce due to traveling storms, *Cont. Shelf Res.*, 11, 139–166, 1991.

Gjevik, B. and Røed, L., Storm surges along the western coast of norway, *Tellus*, 28, 166–182, 1976.

Hackett, B., Røed, L., Gjevik, B., Martinsen, E., and Eide, L., A review of the metocean modeling project (momop), part 2: Model validation study, in *Quantitative Skill Assessment for Coastal Ocean Models*, edited by D. Lynch and A. Davies, American Geophysical Union, 1995.

Hansen, B. and Østerhus, S., North atlantic-nordic seas exchanges, *Progress in Oceanography*, 45, 109–208, 2000.

Haugan, P., Evensen, G., Johannessen, J., Johannessen, O., and Pettersson, L., Modeled and observed mesoscale circulation and wave-current refraction during the 1988 norwegian shelf experiment, *J.Geophys.Res.*, 96, 10487–10506, 1991.

Kurihara, Y. and M.A., B., Use of a movable nested-mesh model for tracking a small vortex, *Mon. Wea. Rev.*, 108, 1792–1809, 1980.

Kurihara, Y., Tripoli, G., and M.A., B., Design of a movable nested-mesh primitive equation model, *Mon. Wea. Rev.*, 107, 239–249, 1979.

Laugier, M., Angot, P., and Mortier, L., Nested grid methods for an ocean model: A comparative study, *Int.J.Numer.Meth.Fluids*, 23, 1163–1195, 1996.

Martinsen, E. and Engedahl, H., Implementation and testing of a lateral boundary scheme as an open boundary condition in a barotropic ocean model, *Coastal Engineering*, 11, 603–627, 1987.

Martinsen, E., Gjevik, B., and Røed, L., A numerical model for long barotropic waves and storm surges along the western coast of Norway, *J.Phys.Oceanogr.*, 9, 1126–1138, 1979.

Mellor, G. and Yamada, T., Development of a turbulence closure model for geophysical fluid problems, *Rev. Geophys. Space Phys.*, 20, 851–875, 1982.

Mesinger, F. and Arakawa, A., Numerical methods used in atmospheric models, Volume I, 1976, WMO/ICSU Joint Organizing Committee, Garp Publication Series No. 17.

Oey, L. and Chen, P., A Nested-Grid Ocean Model: With Application to the Simulation of Meanders and Eddies in the Norwegian Coastal Current, *J. of Geophys. Res.*, 97(C12), 20063–20086, 1992.

Østerhus, S. and Gammelsrød, T., The abyss of the Nordic Seas is warming, *Journal of Climate*, 12, 3297–3304, 1999.

Rowley, C. and Ginis, I., Implementation of a mesh movement sceme in a multiply nested ocean model and its application to air-sea interaction studies, *Monthly Weather Review*, 127, 1879–1896, 1999.

Smagorinsky, J., General circulation experiments with the primitive equations, I. The basic experiment, *Mon. Weather Rev.*, 91, 99–164, 1963.

Spall, M. and Holland, W., A nested primitive equation model for oceanic applications, *J.Phys.Oceanogr.*, 21, 205–220, 1991.

Svendsen, E., Berntsen, J., Skogen, M., Ådlandsvik, B., and Martinsen, E., Model simulation of the Skagerrak circulation and hydrography during SKAGEX, *Journal of Marine Systems*, 8, 219–236, 1996.

Sweby, P., High resolution schemes using flux limiters for hyperbolic conservation laws, *SIAM J. Numer. Anal.*, 21, 995–1011, 1984.

Wang, D.-P., Mutual intrusion of a gravity current and density front formation, *J. Phys. Oceanogr.*, 14, 1191–1199, 1984.

Zhang, D.-L., Chang, H.-R., Seaman, N., Warner, T., and Fritsch, J., A two-way interactive nesting procedure with variable terrain resolution, *Mon. Wea. Rev.*, 114, 1330–1339, 1986.

Depotbiblioteket
01sd 05 803